Supplementary Materials

Zeolitic imidazole framework derived N-doped porous carbon/metal cobalt nanoparticles hybrid for oxygen electrocatalysis and rechargeable Zn−Air battery

Xia Liu,[a] Yuanyuan Ma,[b] Yongliang Cai,[a] Song Hu,[a] Jian Chen,[a] Linzhao Liu[c],* and Zhijuan Wang[a],*

[a]Institute of Advanced Synthesis (IAS), School of Chemistry and Molecular Engineering (SCME), Jiangsu National Synergetic Innovation Center for Advanced Materials (SICAM), Nanjing Tech University, 30 South Puzhu Road, Nanjing 211816, PR China

[b]Department of Materials Science and Engineering, National University of Singapore,117574, Singapore.

[c]Institute of Materials Research and Engineering, Agency for Science, Technology and Research (A*STAR), 2 Fusionopolis Way, #08-03 Innovis 138634, Singapore.
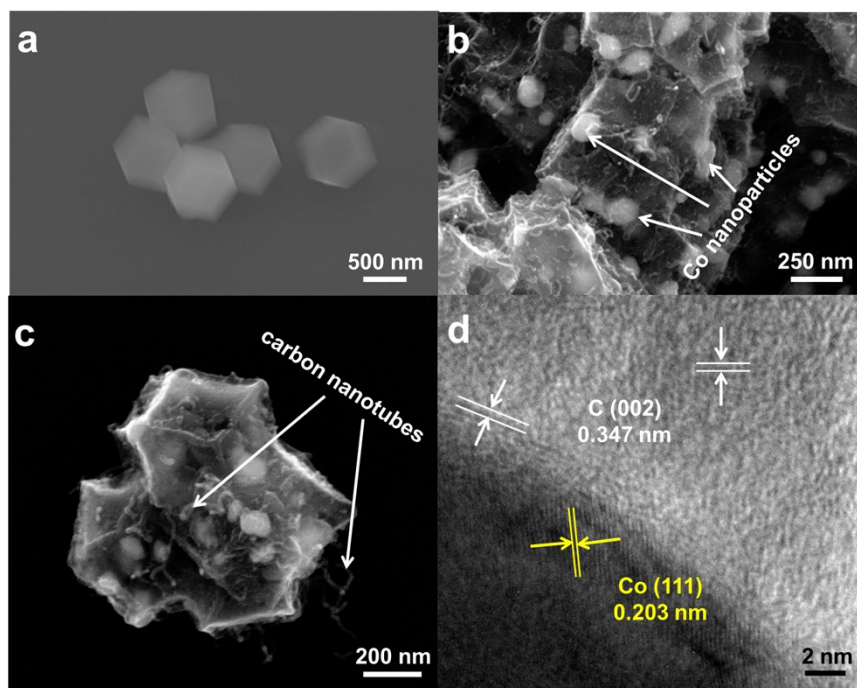
Figure S1. SEM images of ZIF-8@ZIF-67 (1/2) (a) and C-N/Co (1/2) (b, c)，and high-resolution TEM image of C-N/Co (1/2) (d).
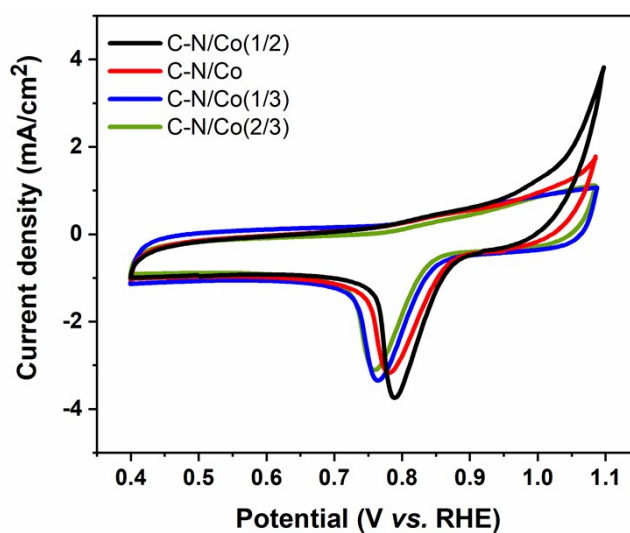

Figure S2. Cyclic voltammograms of the ORR in O_2-saturated 0.1 M KOH solution on the synthesized catalysts.
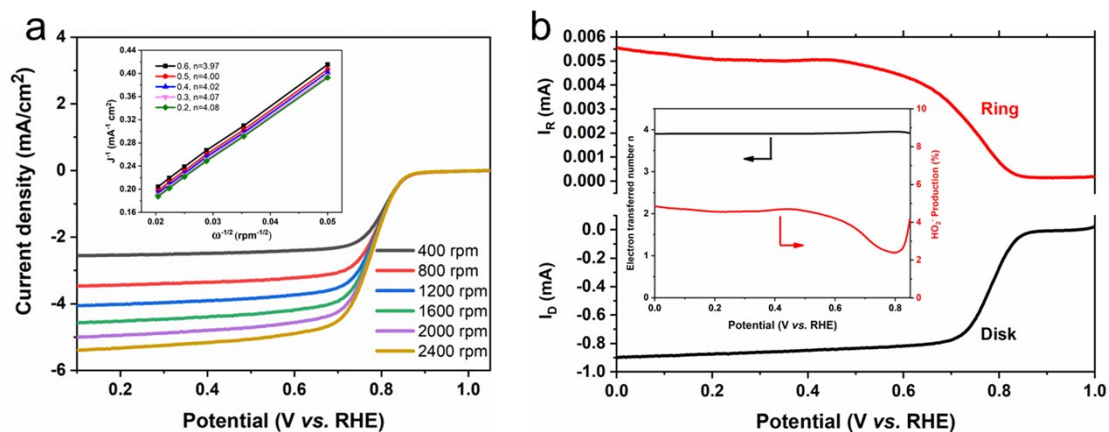
Figure S3. (a) RDE LSV cures of the ORR in O_2-saturated 0.1 M KOH solution on C-N/Co (1/2) at different rotation rates from 400 to 2400 rpm; The inset figure shows the Koutecky-Levich plots for C-N/Co (1/2) at various potentials. (b) Voltammograms of C-N/Co (1/2) measured with rotating ring-disk electrode (RRDE) in O_2-saturated 0.1 M KOH at a rotating rate of 1,600 rpm and a potential scanning rate of 5 mV s^{-1}; The inset shows the corresponding electron transfer number and HO_2^- production yield at various potentials.
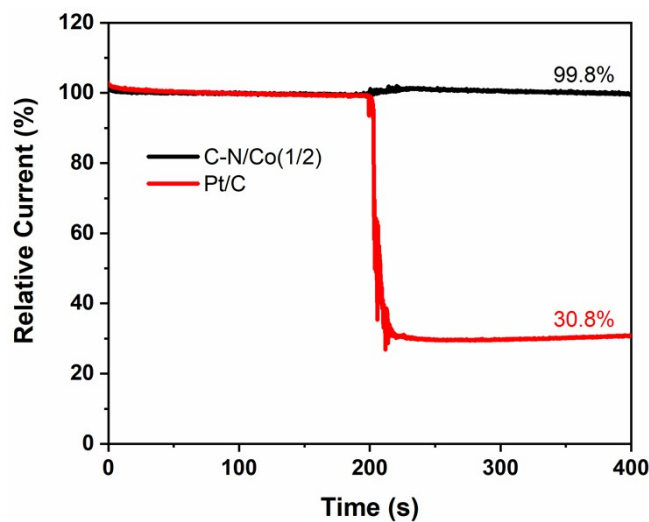

Figure S4. Chronoamperometry test of C-N/Co (1/2) and Pt/C on addition of 1.0 M methanol after about 200 s in O_2-saturated 0.1 M KOH solution at 0.6 V.
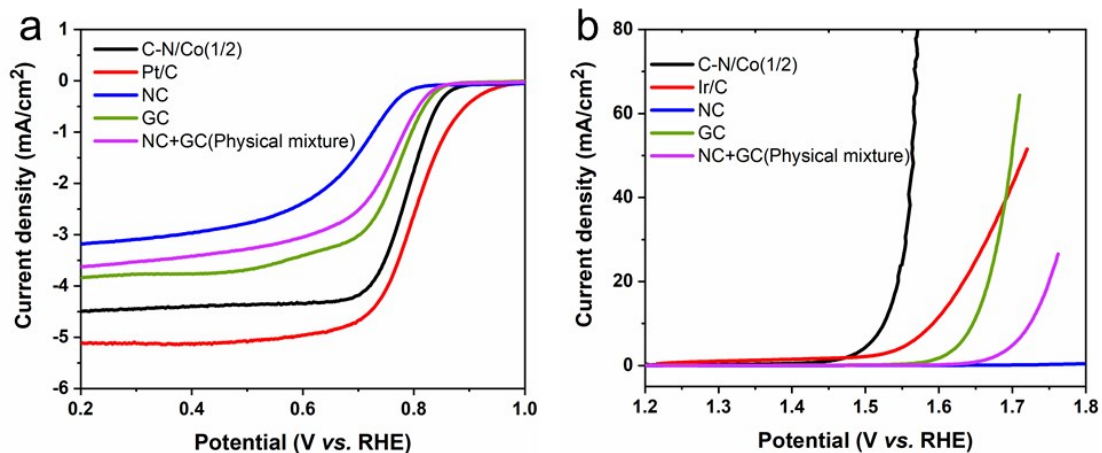
Figure S5. LSV curves of C-N/Co(1/2) and the compared samples in O_2-saturated 0.1 M KOH solution for ORR (a) and in O_2-saturated 1 M KOH solution for OER (b).
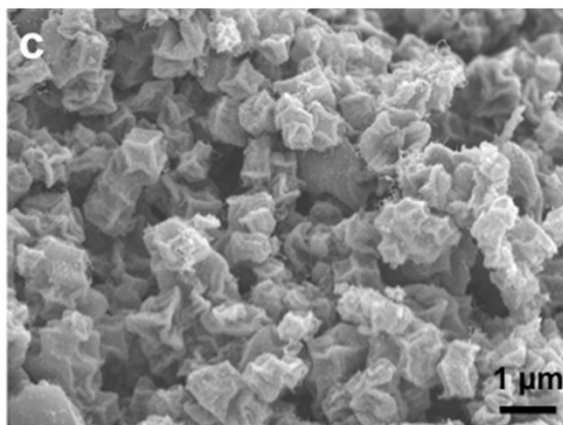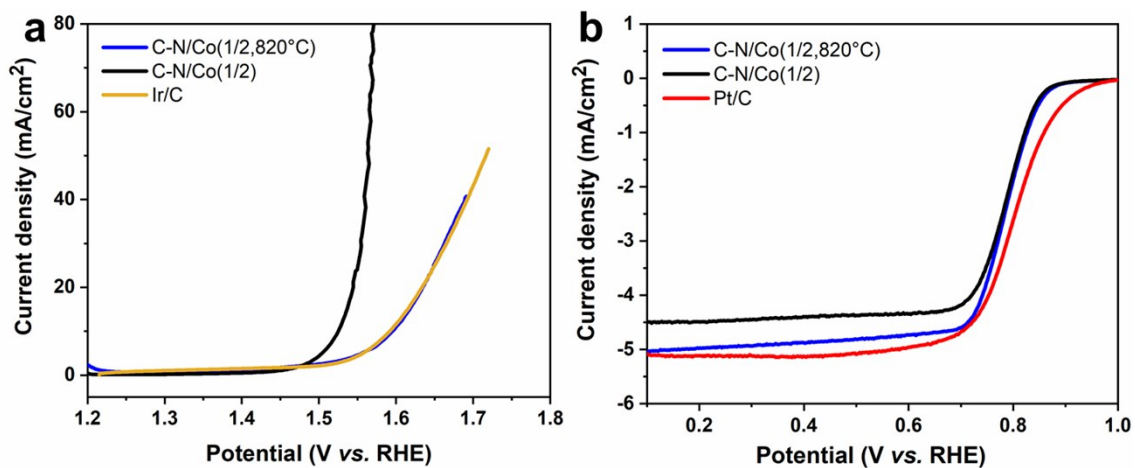

Figure S6. LSV curves of C-N/Co (1/2) carbonized at 820 °C in O_2-saturated 1 M KOH solution for OER (a) and in O_2-saturated 0.1 M KOH solution for ORR (b). SEM image of C-N/Co (1/2) carbonized at 820 °C (c).
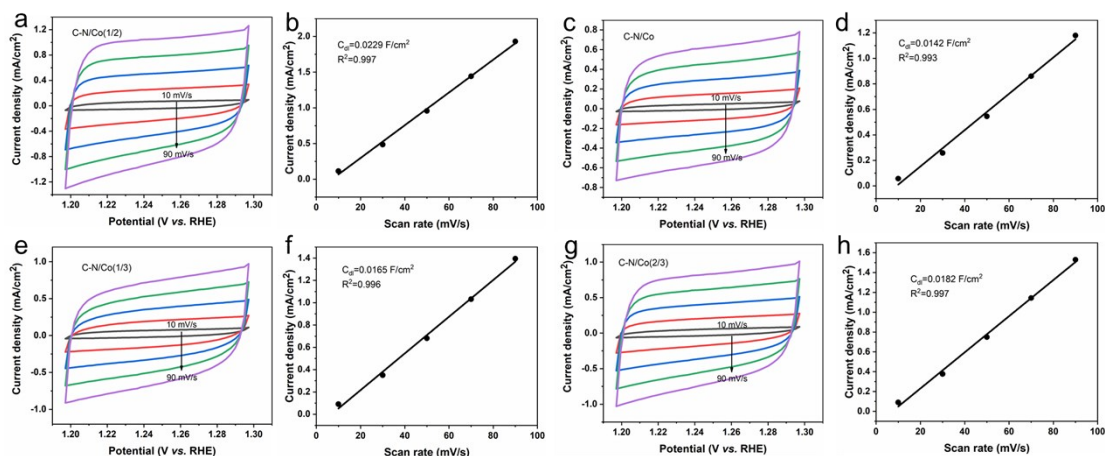
Figure S7. (a, c, e, g) Cyclic voltammograms of the synthesized catalysts at different scanning rates; (b, d, f, h) the corresponding plots of the capacitive current at 1.25 V as a function of the scan rate.

The electrochemical double-layer capacitance (C_{dl}) was measured via performing cyclic voltammetry (CV) in the illegal Faraday electrode potential range with different scan rates. Because the electrochemical active surface area (ECSA) is proportional to the C_{dl}, C_{dl} is often used to estimate the ECSA [1, 2]. As can be seen from Fig.S7, the potential range of the measured samples was 1.20~1.3 V and the scanning speeds was between 10 and 90 mV s^{-1} with an interval of 20 mV s^{-1} in this study. The C-N/Co (1/2) composite manifests larger C_{dl} (22.9 mF cm^{-2}) than C-N/Co (14.2 mF cm^{-2}), C-N/Co (1/3) (16.5 mF cm^{-2}) and C-N/Co (2/3) (18.2 mF cm^{-2}). It is recognized that an increase of ECSA leads to the enhancement of catalytic activity [3]. Therefore, increased electrochemically active sites are exposed on the surface of C-N/Co (1/2) catalyst in consideration of the similar BET specific surface areas of as-prepared composites.
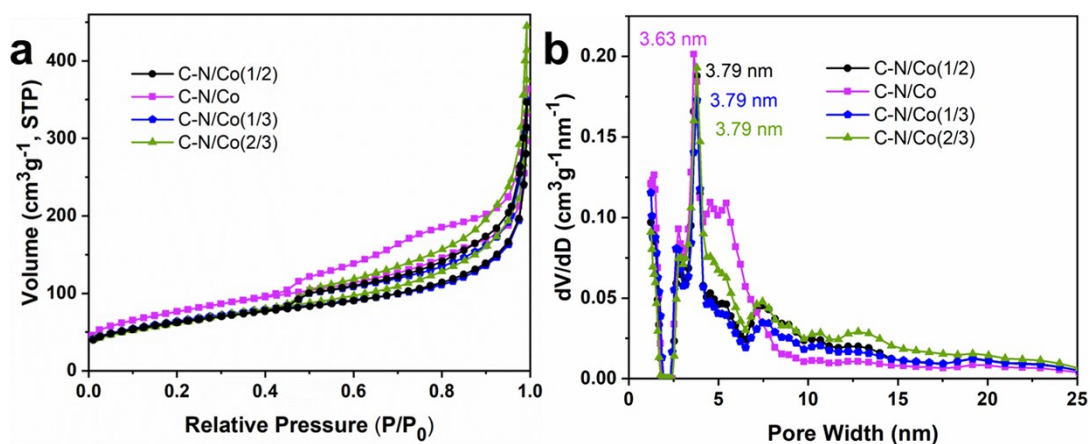
Figure S8. (a) N_2 adsorption-desorption isotherms and (b) the pore size distributions of the synthesized catalysts.

Nitrogen adsorption-desorption isotherm measurements were used to analyze the specific surface area and pore size distribution of the samples. As shown in Fig.S2a, all N_2 adsorption-desorption isotherms demonstrate a typical type-IV isotherm, suggesting the presence of a mesoporous structure. Normally, the larger specific surface area is anticipated to supply more active sites, leading to a better electrochemical activity. However, the Brunauer-Emmett-Teller (BET) surface area of the C-N/Co (1/2) was 224.5 $m^2\ g^{-1}$, which is similar to that of the C-N/Co (275.5 m^2 g^{-1}), C-N/Co (1/3) (228.7 $m^2\ g^{-1}$) and C-N/Co (2/3) (223.9 $m^2\ g^{-1}$). This is different from the ORR (Fig. 5b) and OER (Fig. 5d) results, indicating the BET specific surface area may be not the main reason that affects the electrocatalytic properties of the catalyst in this system. Besides, the porous structure and carbon nanotubes endow all synthesized composites large specific surface areas, being supposed to be conducive to electron and mass transport[4-6]. Fig.S2b shows the relative Barrett-Joyner-Halenda (BJH) pore size was distributed at ~3.79 nm and further confirms the

mesoporous structure of C-N/Co (1/2).

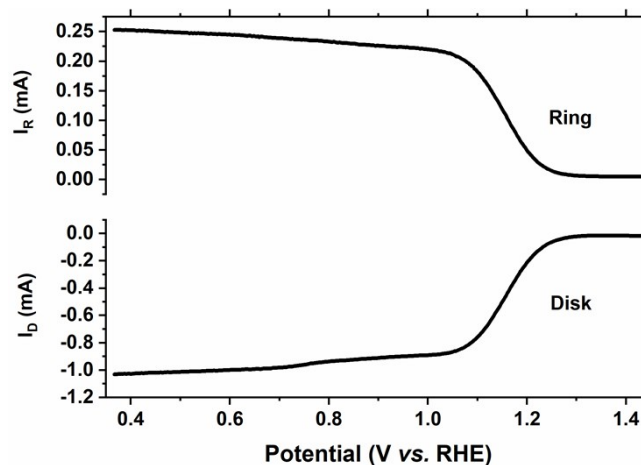**Figure S9.** Ring ($Fe^{2+} \rightarrow Fe^{3+} + e^-$) and disk ($Fe^{3+} + e^- \rightarrow Fe^{2+}$) currents for the determination of collection efficiency of RRDE loaded with C-N/Co (1/2) catalyst. The electrolyte is degassed 0.1 M NaOH with 0.01 M $K_3Fe(CN)_6$. The rotating rate of RRDE is 1600 rpm and a potential scanning rate is 5 mV s^{-1}. The collection efficiency is calculated to be $(24.6 \pm 0.3)\%$, close to the manufactures data 24.9%.

Table S1. Comparison of ORR performance of C-N/Co (1/2) with other electrocatalysts reported in literature.

Catalysts	Onset potential (V)	n	Electrolyte
C-N/Co (1/2) (this work)	0.89	3.96	0.1 M KOH
300nm-MDC[7]	0.86	3.7	0.1 M HClO$_4$
CoNi-MOF/rGO[8]	0.88		0.1 M KOH
O-NiCoFe-LDH[9]	0.8	3.9	0.1 M KOH
meso-Co$_3$O$_4$-35[10]	0.75	3.5~3.9	0.1 M KOH
Carbon-L[11]	0.86	3.68	0.1 M KOH
CoP@SNC[12]	0.87	3.82~3.99	0.1 M KOH
CNF@Zn/CoNC[13]	0.91	>3.88	0.1 M KOH
CNF@CoNC[13]	0.89	>3.8	0.1 M KOH
CoP NCs[14]	0.8	3.5	0.1 M KOH

Table S2. Comparison of OER performance of C-N/Co (1/2) with other electrocatalysts reported in literature.

Catalysts	η at 10 mA cm^{-2} (V)	Tafel slope (mV dec^{-1})	Electrolyte
C-N/Co (1/2) (this work)	0.29	66	1 M KOH
CoNi-MOF/rGO[8]	0.318	48	1 M KOH
O-NiCoFe-LDH[9]	0.34	93	0.1 M KOH
meso-Co_3O_4-35[10]	0.411	80	0.1 M KOH
CoP@SNC[12]	0.35	68	1 M KOH
CNF@Zn/CoNC[13]	0.47	124	0.1 M KOH
CNF@CoNC[13]	0.48	147	0.1 M KOH
Zn-doped $CoSe_2$/CFC[15]	0.356	88	1 M KOH
CoP/rGO[16]	0.34	66	1 M KOH
CoS_2 NTA[17]	0.276	81	1 M KOH

References

1   C. Feng, Y. Guo, Y. H. Xie, X. L. Cao, S. Li, L. G. Zhang, W. Wang and J. Wang, *Nanoscale.*, 2020, **12**, 5942-5952.

2   L. Yan, L. Cao, P. Dai, X. Gu, D. Liu, L. Li, Y. Wang and X. Zhao, *Adv. Funct. Mater.*, 2017, **27**, 1703455.

3   T. Zhang, J. Du, P. X. Xi and C. L. Xu, *ACS Appl. Mater. Interfaces.*, 2017, **9**, 362–370.

4   S. Dou, X. Y. Li, L. Tao, J. Huo and S. Y. Wang, *Chem. Commun.*, 2016, **52**, 9727-9730.

5   J. S. Meng, C. J. Niu, L. H. Xu, J. T. Li, X. Liu, X. P. Wang, Y. Z. Wu, X. M. Xu, W. Y. Chen, Q. Li, Z. Z. Zhu, D. Y. Zhao and L. Q. Mai, *J. Am. Chem. Soc.*, 2017, **139**, 8212–8221.

6   Z. Q. Liu, H. Cheng, N. Li, T. Y. Ma and Y. Z. Su, *Adv. Mater.*, 2016, **28**, 3777-3784.

7   W. Xia, J. Zhu, W. Guo, L. An, D. Xia and R. Zou, *J. Mater. Chem. A.*, 2014, **2**, 11606-11613.

8   X. Zheng, Y. Cao, D. Liu, M. Cai, J. Ding, X. Liu, J. Wang, W. Hu and C. Zhong, *ACS Appl. Mater. Interfaces.*, 2019, **11**, 15662-15669.

9   L. Qian, Z. Lu, T. Xu, X. Wu, Y. Tian, Y. Li, Z. Huo, X. Sun and X. Duan, *Adv. Energy Mater.*,

2015, **5**, 1500245.

10   Y. J. Sa, K. Kwon, J. Y. Cheon, F. Kleitz and S. H. Joo, *J. Mater. Chem. A.*, 2013, **1**, 9992-10001.

11   P. Zhang, F. Sun, Z. Xiang, Z. Shen, J. Yun and D. Cao, *Energy Environ. Sci.*, 2014, **7**, 442-450.

12   T. Meng, Y.-N. Hao, L. Zheng and M. Cao, *Nanoscale.*, 2018, **10**, 14613–14626.

13   Y. X. Zhao, Q. X. Lai, J. J. Zhu, J. Zhong, Z. M. Tang, Y. Luo and Y. Y. Liang, *Small.*, 2018, **14**, 1704207.

14   H. C. Yang, Y. J. Zhang, F. Hu and Q. B. Wang, *Nano Lett.*, 2015, **15**, 7616-7620.

15   Q. C. Dong, Q. Wang, Z. Y. Dai, H. J. Qiu and X. C. Dong, *ACS Appl. Mater. Interfaces.*, 2016, **8**, 26902-26907.

16   L. Jiao, Y.-X. Zhou and H.-L. Jiang, *Chem. Sci.*, 2016, **7**, 1690-1695.

17   C. Guan, X. M. Liu, A. M. Elshahawy, H. Zhang, H. J. Wu, S. J. Pennycook and J. Wang, *Nanoscale Horiz.*, 2017, **2**, 342-348.